Available online at www.sciencedirect.com
SCIENCE DIRECT®
Journal of Sound and Vibration 282 (2005) 1065–1083
JOURNAL OF SOUND AND VIBRATION
www.elsevier.com/locate/jsvi

Stability analysis of rotating blade bending vibration due to torsional excitation

B.O. Al-Bedoor[1], A.A. Al-Qaisia*

Faculty of Engineering and Technology, Mechanical Engineering Department, University of Jordan, Amman 11942, Jordan

Received 18 November 2003; accepted 22 March 2004
Available online 12 October 2004

Abstract

This paper studies the forced vibrations of a flexible rotating blade under the excitation of shaft torsional vibration. A reduced order nonlinear dynamic model is adopted, wherein the torsional vibration degree of freedom is substituted by a simple harmonic motion with a frequency that is function of the system rotating speed. The resulting system of second-order ordinary differential equation with harmonically varying coefficients is solved using the method of harmonic balance. The forced response solution is compared to the numerical integration results. Agreement is found with respect to stable and unstable regions of the blade vibrations. The solution is useful for defining dangerous operating speed ranges and for quantifying the relationship between shaft torsional and blade bending natural frequencies.
© 2004 Elsevier Ltd. All rights reserved.

1. Introduction

Rotating blade vibration was recognized as one major cause of failure in turbomachinery that put a growing demand on more thorough analysis at the design stage. One problem that deserves more attention is the problem of blade vibration instability due to torsional vibration excitation.

*Corresponding author. Tel.: +962-6-5355000 × 2783; fax: +962-6-5355-588.
E-mail address: alqaisia@ju.edu.jo (A.A. Al-Qaisia).
[1]On leave from King Fahd University of Petroleum and Minerals, Dhahran, Saudi Arabia.

0022-460X/$ - see front matter © 2004 Elsevier Ltd. All rights reserved.
doi:10.1016/j.jsv.2004.03.038

Consequently, a study that produces a tool for stability analysis is urgently needed not only for design purposes but also for diagnostic studies.

The importance of blade vibration was highlighted by Srinivasan [1] in his survey on the vibration of bladed disk assemblies. He classified blade vibrations into two categories; namely structure induced vibration and aero-elastic induced vibrations. More attention of the survey was given to the structure induced vibration and their modeling. The effects of rotor flexural dynamics on the rotating blade vibration were reported by a number of investigators [2–4]. The problem, of blade vibration and its interaction with the main rotor torsional vibration was studied by Okabe et al. [5]. They showed that it is necessary to model both blade bending vibration and main rotor torsional vibration in turbomachinery. They employed an equivalent reduced order model that coupled the blade tangentional vibration and the shaft torsional vibrations. Their model adopted the modal synthesis procedure, wherein the blade was modeled as a simple mass-spring subsystem and the shaft torsional flexibility as another discrete subsystem. The two subsystems were coupled and the natural frequencies were analyzed. The model-produced natural frequencies were compared to the actual measurement and close agreement was reported. Huang and Ho [6] reported results of a study on the coupled shaft torsional and blade bending vibrations of a rotating shaft-disk-blade unit. The shaft torsional and blade bending deformations were modeled, separately, using the assumed modes method (AMM). They used the weighted residual method to discretize blade vibration and the receptance at the connection between the disk and the blade to couple the shaft torsional and blade bending dynamics. Al-Bedoor [7], based on the multi-body dynamics approach, developed a coupled model for shaft torsional and blade bending vibrations in rotors. The model employed the finite element method to discretize the blade deformations. The study identified nonlinear interaction that the blade and the shaft introduce to each other. Due to the difficulty encountered in quantifying the nature of nonlinear coupling when the finite element method is used, a reduced-order dynamic model was reported by Al-Bedoor [8]. This model adopted the AMM for approximating the blade deformations. The model was further analyzed for blade vibration under the effect of shaft torsional vibration excitation by Al-Nassar and Al-Bedoor [9]. The blade modal vibration model was extracted from the general model [8], wherein, a Hill's type equation was obtained by assuming small torsional vibrations. The homogeneous part of the Hill's equation was numerically integrated for a combination of blade natural frequencies and torsional vibration excitation frequency. The analysis showed that blade unstable vibration occurs for certain torsional vibration frequencies as related to blade bending natural frequencies. The analysis of Ref. [9] was limited to numerical integration of the homogeneous equation and stable and unstable regions were not explicitly identified. Recently, Al-Bedoor and Al-Qaisia [10] employed the harmonic balance (HB) method solution for finding the steady-state solution of the rotating blade excited by shaft torsional vibrations. A special case was addressed which is the rotating speed torsional excitation, 1X, with small torsional vibration amplitude. Moreover, the solution was obtained using integer numbers for the harmonic analysis that produced discrepancy between the numerical integration solution and the predicted steady-state solution.

This paper is devoted towards finding the steady-state solution of the rotating blade vibration under shaft torsional excitation. The model of Ref. [8] is adopted with no imposed conditions

neither on the strength of the torsional vibration nor on the torsional vibration excitation frequency. The generalized method of HB is employed in finding the steady-state solutions in which the assumed solution contains integers and fractal frequencies. The steady-state solution coefficient matrix eigenvalues are found for stability purposes. Stable and unstable regions are found as a function of operational and design parameters and presented in map format. Numerical integration is used to check the predicted HB solutions.

2. The governing equation

The dynamic model of a blade-disk-shaft system reported by Al-Bedoor [8] and shown in Fig. 1 is used in this study. The equation of blade modal vibration can be written in the form

$$m_{q\theta}\ddot{\theta} + m_{q\psi}\ddot{\psi} + m_{qq}\ddot{q} + C_{q\theta}\dot{\theta} + C_{qq}\dot{q} + k_{qq}q = F_q, \tag{1}$$

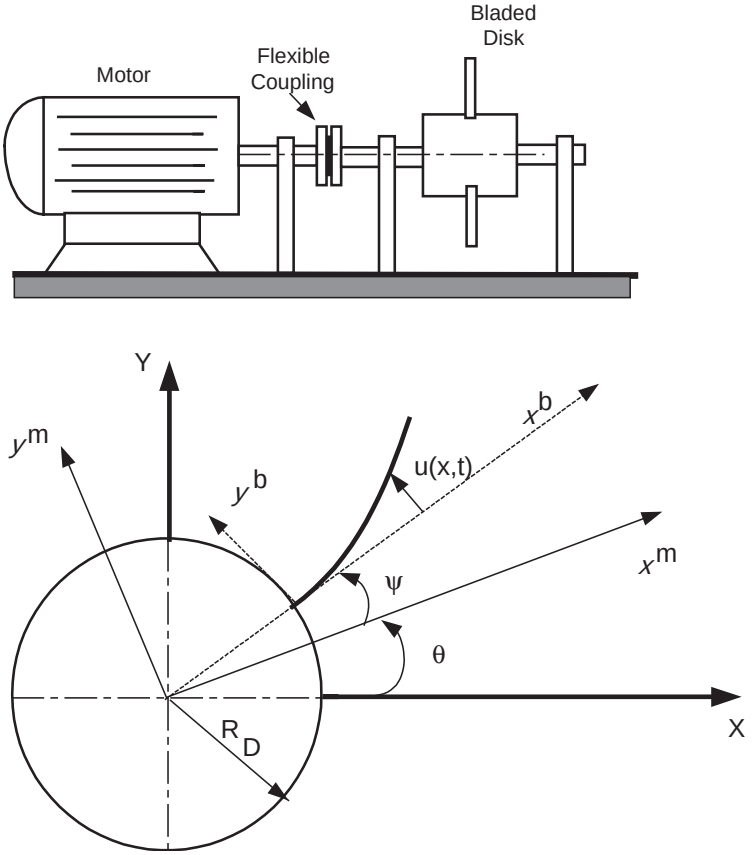

Fig. 1. Schematic of the rotor-disk-blade system and coordinates system.

Table 1
Blade parameters

Length, L	0.4 m
Mass/length, ρ	1.35 kg/m
Flexural rigidity, EI	75 N m^2
Disk radius, r_D	0.05 m

Table 2
Modal parameters

k_{s1}	k_{s2}	a	b	k_i
1.57088	2.38667	0.568826	0.78992	12.3624
8.6471	12.9565	0.0907	0.43396	485.52
24.95	35.71	0.032416	0.2544	3806.55
51.45	72.11	0.01654	0.1818	14617.2

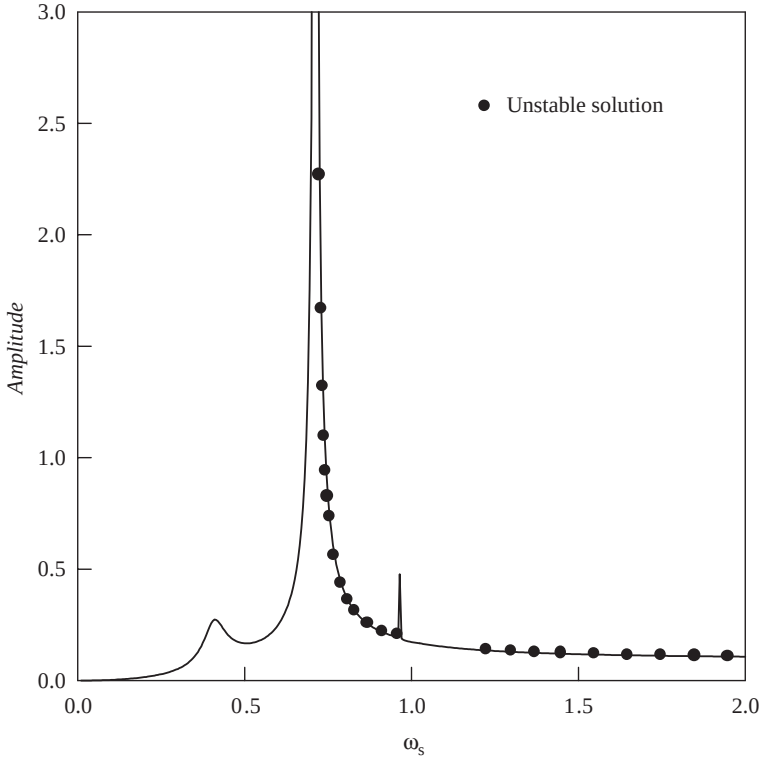

Fig. 2. SSFR of the blade first mode. $\varepsilon = 1$, $\gamma = 1$, $\zeta = 0.1$. ———SSFR; ● unstable points on SSFR.

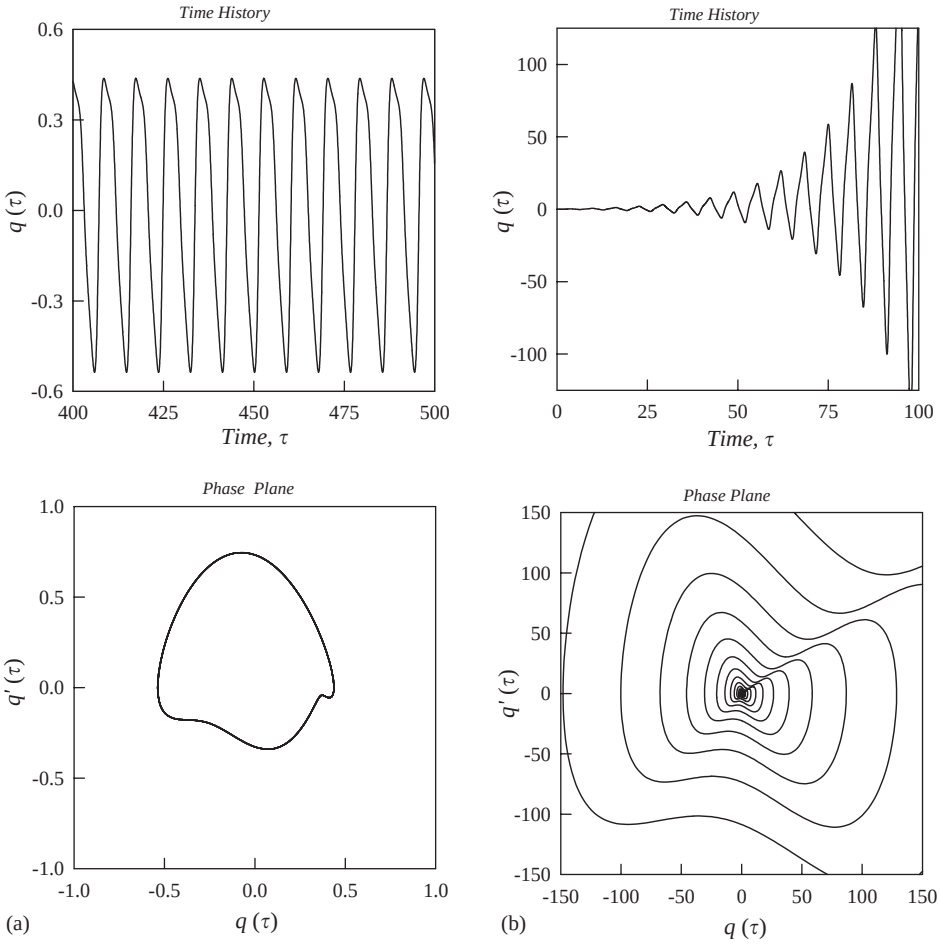

Fig. 3. Time history and phase plane of the first mode. $\varepsilon = 1$, $\gamma = 1$, $\zeta = 0.1$. (a) $\omega_s = 0.71$ and (b) $\omega_s = 0.96$.

where θ is the rigid body rotation, ψ is the torsional deformation angle and q is the blade bending modal deformation. The coefficients of Eq. (1) obtained from the model are

$$a = \int_0^L \rho x \phi(x)\,\mathrm{d}x,$$

$$b = \int_0^L \rho \phi(x)\,\mathrm{d}x,$$

$$k_{s1} = \int_0^L \rho(L - x)\phi'^2(x)\,\mathrm{d}x,$$

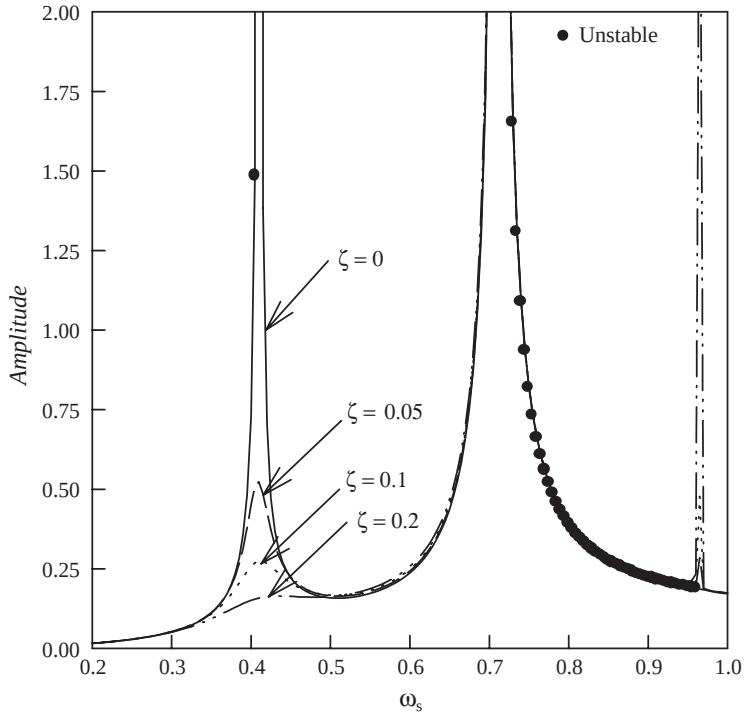

Fig. 4. Effect of damping on SSFR of the first mode. ● unstable points on SSFR.

$$k_{s2} = \int_0^L \rho(L-x)^2 \phi'^2(x)\,\mathrm{d}x,$$

$$k_i = \int_0^L \phi''^2(x)\,\mathrm{d}x,$$

$$m_{q\theta} = (1+\psi^2)h,$$

$$m_{q\psi} = h + \psi q,$$

$$m_{qq} = 1 + \psi^2,$$

$$C_{q\theta} = 2\psi\dot{\psi}h,$$

$$C_{qq} = 2\psi\dot{\psi},$$

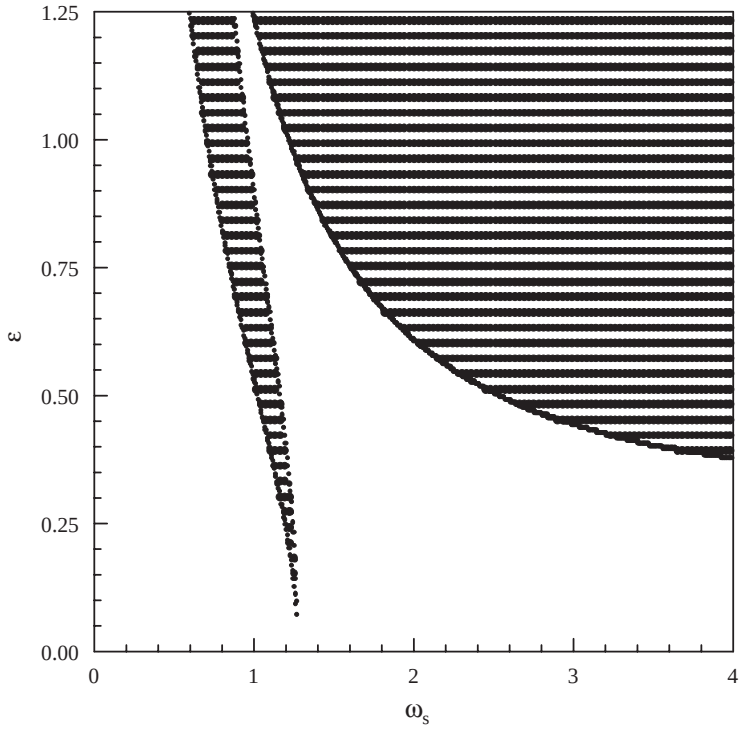

Fig. 5. Stability chart of the first mode blade bending vibrations: $\gamma = 1$, $\zeta = 0.1$, shaded areas are unstable.

$$k_{qq} = \frac{\mathrm{EI}}{\rho L^4} k_i + (\dot{\theta} + \dot{\psi})^2 [k_s - 1] + \dot{\psi}^2 - \psi^2 \dot{\theta}^2,$$

$$h = a + R_D b,$$

$$k_s = R_D k_{s1} + \tfrac{1}{2} k_{s2}, \tag{2}$$

where ρ is the blade mass per unit length, $\phi(x)$ is the shape function of a cantilever beam, EI is the flexural rigidity, L is the blade length and R_D is the disk radius.

For the system that is rotating at constant speed, $\dot{\theta} = \omega$, the term that contains the second derivative of the rigid body rotation $\ddot{\theta}$ in Eq. (1) can be dropped. Moreover, the torsional vibration can be assumed to occur at single frequency that is usually related to the shaft running speed ω as follows:

$$\psi = \varepsilon \sin \gamma \omega t, \tag{3}$$

where ε is constant that controls the magnitude of torsional vibration and γ is the ratio of torsional vibration frequency to the running speed ω.

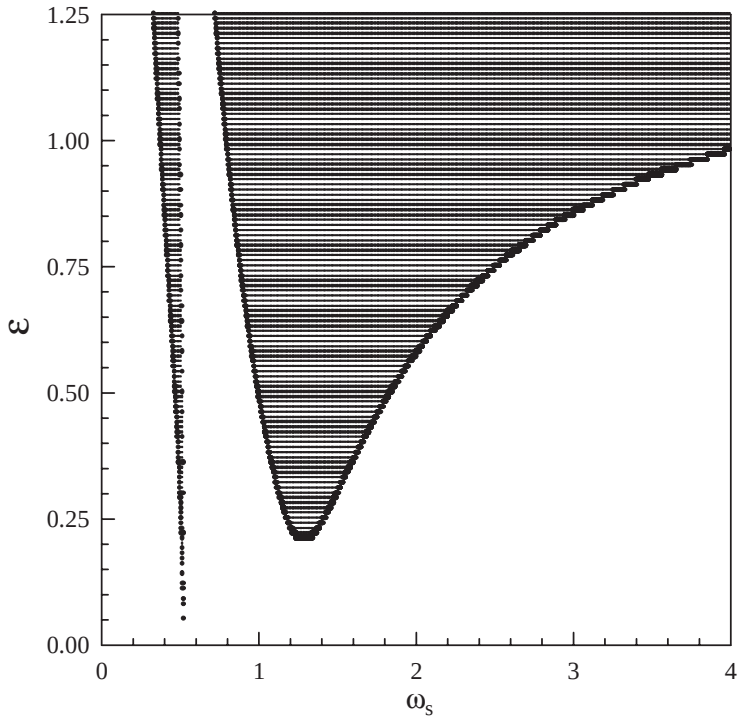

Fig. 6. Stability chart of the first mode blade bending vibrations. $\gamma = 2$, $\zeta = 0.1$, shaded areas are unstable.

Now substituting for ψ and its derivatives into Eq. (1), and defining a new constant $C = k_s - 1$, the rotating blade modal vibrations can be expressed as

$$\begin{aligned}(1 + \varepsilon^2 \sin^2 \gamma\omega t)\ddot{q} + (2\omega_B\zeta + 2\varepsilon^2\gamma\omega \sin \gamma\omega t \cos \gamma\omega t)\dot{q} \\ + \{\omega_B^2 + C\omega^2(1 + 2\varepsilon\gamma \cos \gamma\omega t) - \varepsilon^2\omega^2(\gamma^2 + 1)\sin^2 \gamma\omega t + \varepsilon^2\gamma^2\omega^2(C + 1)\cos^2 \gamma\omega t\}q \\ = h\omega^2\varepsilon\gamma(\gamma \sin \gamma\omega t - 2\varepsilon \sin \gamma\omega t \cos \gamma\omega t),\end{aligned} \tag{4}$$

where $\omega_B^2 = \sqrt{(\mathrm{EI}/\rho L^4)k_i}$ is the blade bending natural frequency, ω is the running speed and γ is the torsional vibration excitation frequency factor.

3. Analysis

The blade steady-state frequency response (SSFR) due to the shaft torsional vibration excitations is presented using the method of HB. After introducing a new dimensionless time scale related to the blade bending natural frequency, $\tau = \omega_B t$ and defining the frequency ratio

$\omega_s = \omega/\omega_B$, Eq. (4) can be re-written as follows:

$$\left(1 + \frac{\varepsilon^2}{2}(1 - \cos 2\gamma\omega_s\tau)\right)q'' + (2\zeta + \varepsilon^2\gamma\omega_s \sin 2\gamma\omega_s\tau)q' + \left[1 + \frac{\omega_s^2}{2}\{(2C - \varepsilon^2 + C\varepsilon^2\gamma^2) + 4C\varepsilon\gamma \cos \gamma\omega_s\tau\} + \frac{\omega_s^2}{2}\varepsilon^2(1 + 2\gamma^2 + C\gamma^2)\cos 2\omega_s\tau\right]q = h\omega_s^2\varepsilon\gamma(\gamma \sin \gamma\omega_s\tau - \varepsilon \sin 2\gamma\omega_s\tau) \quad (5)$$

where prime denote derivative with respect to τ. Eq. (5) contains two types of excitations: parametric and external with frequencies ω_s and $2\omega_s$. According to Floquet theorem, a system that is parametrically driven at frequency Ω exhibits resonance whenever $\Omega \cong 2\sqrt{\lambda_0}/i$, where i is an integer and λ_0 is the oscillator natural frequency. In this case, the two driving frequencies are $\Omega_1 = \omega_s$ and $\Omega_2 = 2\omega_s$. Therefore the two combined frequencies produce a parametric resonance

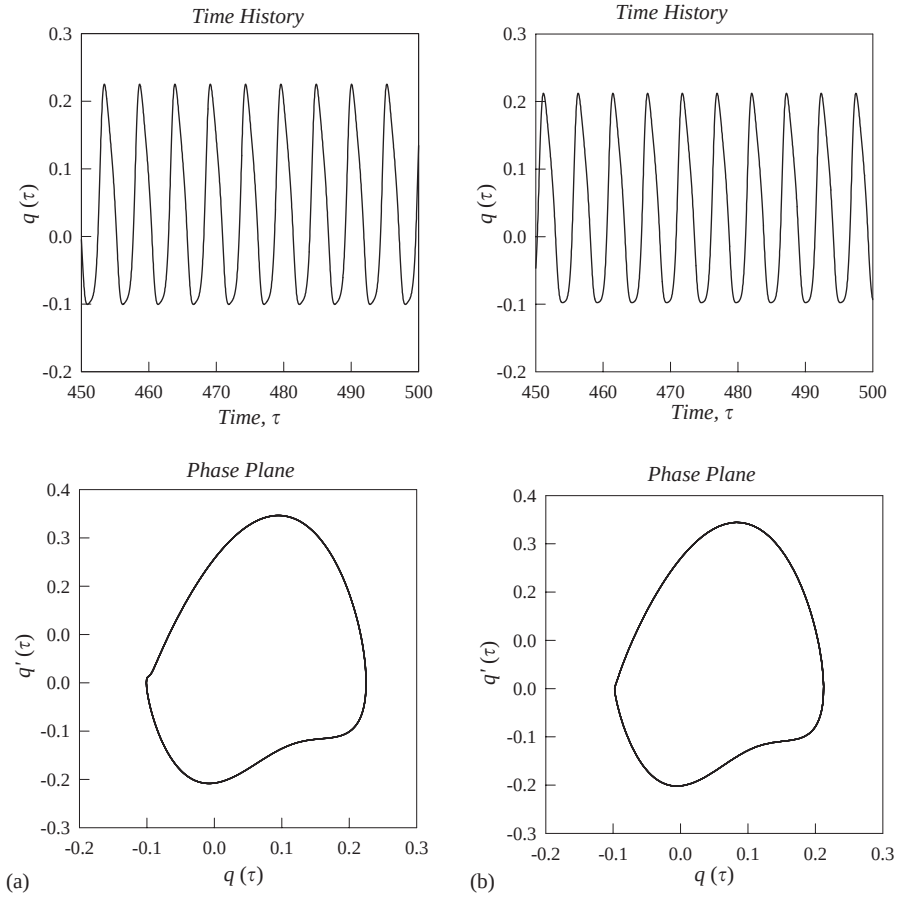

Fig. 7. Time history and phase plane of the first mode. $\zeta = 0.1$. (a) $\varepsilon = 1$, $\gamma = 1$, $\omega_s = 1.2$; (b) $\varepsilon = 1$, $\gamma = 1$, $\omega_s = 1.22$. (c) $\varepsilon = 1.2$, $\gamma = 1$, $\omega_s = 1.0$; (d) $\varepsilon = 0.65$, $\gamma = 1$, $\omega_s = 2.0$. (e) $\varepsilon = 0.6$, $\gamma = 1$, $\omega_s = 2.0$; (f) $\varepsilon = 0.8$, $\gamma = 2$, $\omega_s = 0.8$; (g) $\varepsilon = 0.9$, $\gamma = 2$, $\omega_s = 0.80$ and (h) $\varepsilon = 0.9$, $\gamma = 2$, $\omega_s = 0.85$.

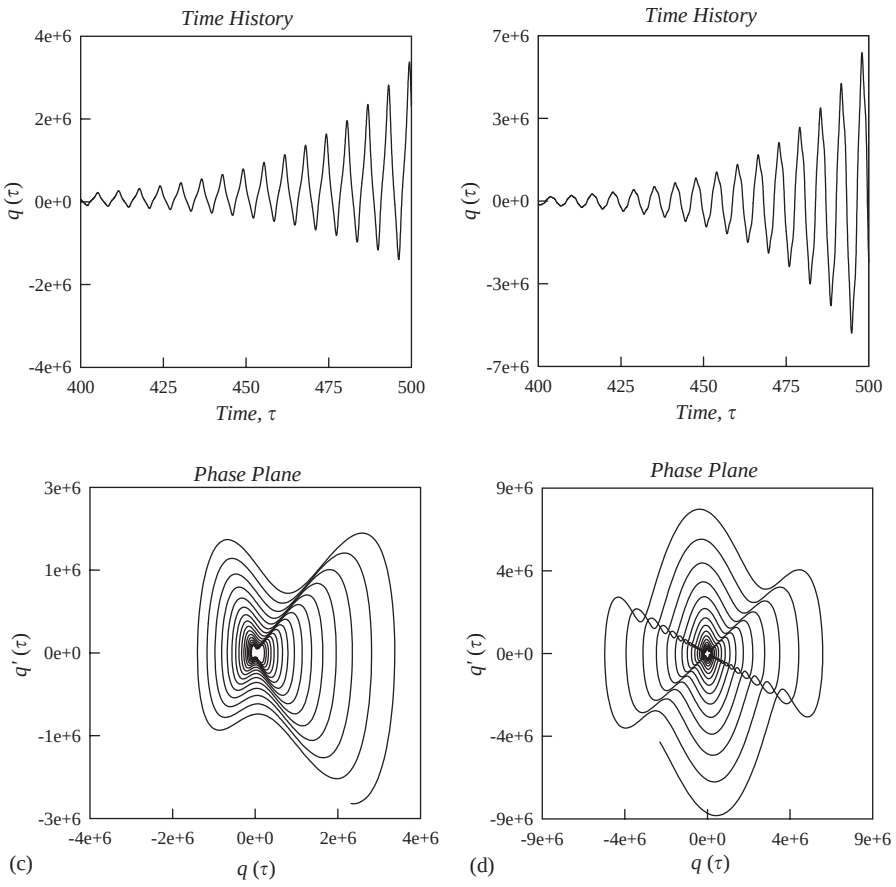

Fig. 7. (*Continued*)

whenever $\omega_s \approx 2\sqrt{\lambda_0}, \sqrt{\lambda_0}, \frac{1}{2}\sqrt{\lambda_0}$, where λ_0 is the normalized natural frequency, which is chosen as 1 in this study.

According to the method of HB, an approximate solution to Eq. (5) can be assumed as a truncated Fourier series, with its contents dictated by the excitation frequencies as follows:

$$q(\tau) = \sum_{n=0}^{N} A_{n/2} \cos(n\gamma\omega_s\tau/2) + B_{n/2} \sin(n\gamma\omega_s\tau/2), \tag{6}$$

where $A_{n/2}$ and $B_{n/2}$ are the amplitudes of the assumed harmonics, that are going to be evaluated based on the method of HB.

As a characteristic of the method of HB, when used for solving parametrically excited system, the most dominant harmonics are not known in advance and the solution first need to be assumed with the broadest possible harmonics. The coefficients are usually evaluated and the ones with almost zero amplitude are ignored. For the present analysis, the dominant harmonics are found,

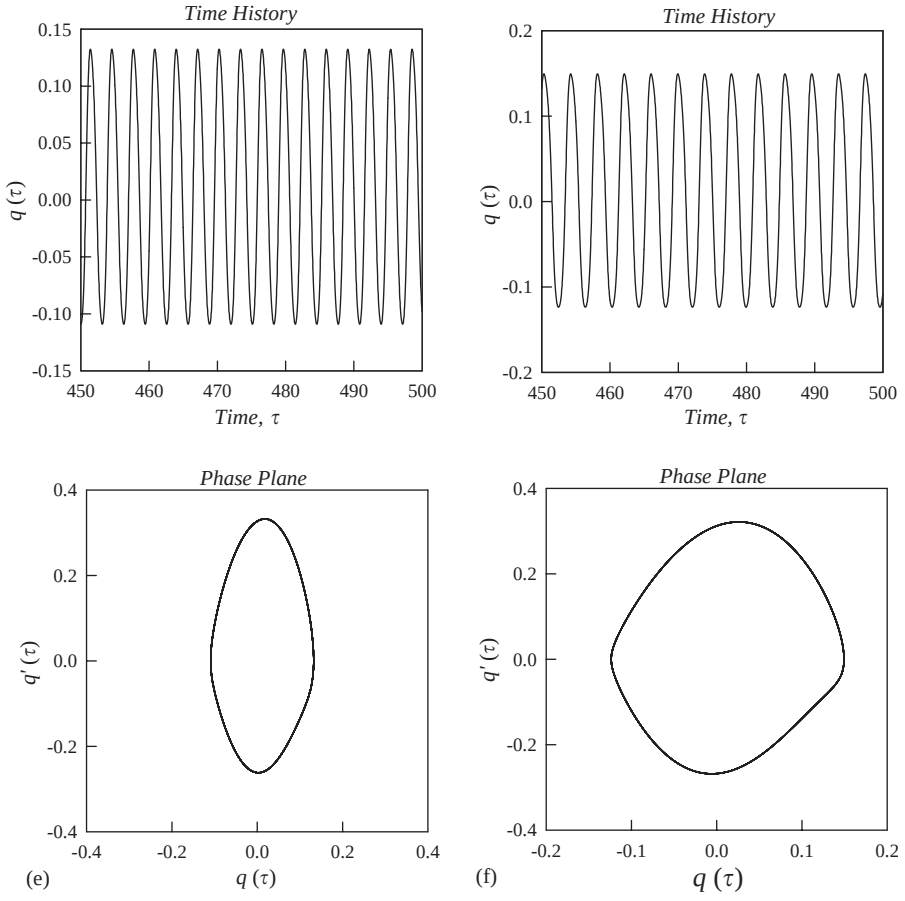

Fig. 7. (*Continued*)

after a number of trials, as in the following assumed solution:

$$q(\tau) = A_0 + A_{1/2}\cos(\gamma\omega_s\tau/2) + B_{1/2}\sin(\gamma\omega_s\tau/2) + A_1\cos\gamma\omega_s\tau + B_1\sin\gamma\omega_s\tau + A_2\cos 2\gamma\omega_s\tau + B_2\sin 2\gamma\omega_s\tau. \quad (7)$$

Substituting Eq. (7) and its derivatives into Eq. (5), and equating the coefficients of similar harmonics a set of algebraic equations are obtained as can be represented in the following matrix form:

$$\mathbf{Mx} = \mathbf{y}, \quad (8)$$

where the vector $\mathbf{x}^{\mathrm{T}} = \{A_0, A_{1/2}, B_{1/2}, A_1, B_1, A_2, B_2\}$, $\mathbf{y}^{\mathrm{T}} = \{0, 0, 0, 0, h\varepsilon(\gamma\omega_s)^2, 0, -h\gamma(\varepsilon\omega_s)^2\}$ and the non-zero entries of the (7×7) coefficient matrix $\mathbf{M}$ are as follows:

$$M_{11} = 1 + \frac{\omega_s^2}{2}(2C - \varepsilon^2 + C\varepsilon^2\gamma^2),$$

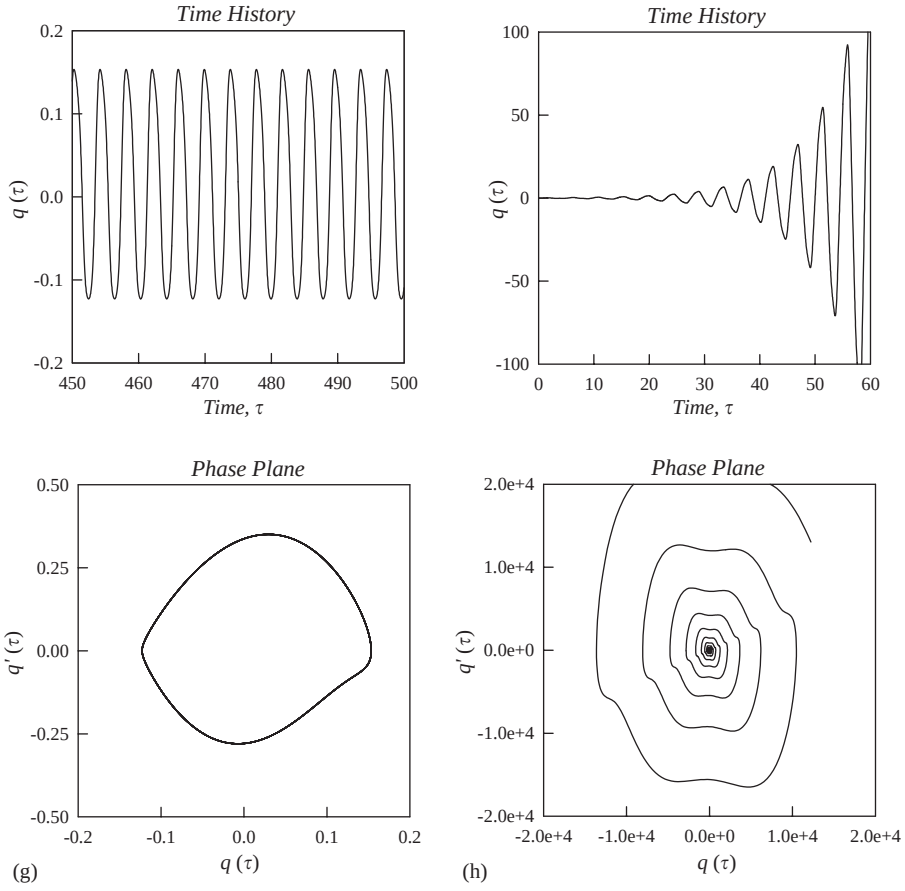

Fig. 7. (*Continued*)

$$M_{14} = C\varepsilon\gamma\omega_s^2,$$

$$M_{16} = \frac{\varepsilon^2}{4}\,\omega_s^2(1 + \gamma^2(2 + C),$$

$$M_{22} = 1 + \frac{\omega_s^2}{8}\,\{4C(2 + 2\varepsilon\gamma + \varepsilon^2\gamma^2) - (4\varepsilon^2 + 2\gamma^2 + \varepsilon^2\gamma^2)\},$$

$$M_{23} = \gamma\zeta\omega_s,$$

$$M_{32} = -M_{23},$$

$$M_{33} = 1 + \frac{\omega_s^2}{8}\,\{4C(2 - 2\varepsilon\gamma + \varepsilon^2\gamma^2) - (4\varepsilon^2 + 2\gamma^2 + \varepsilon^2\gamma^2)\},$$

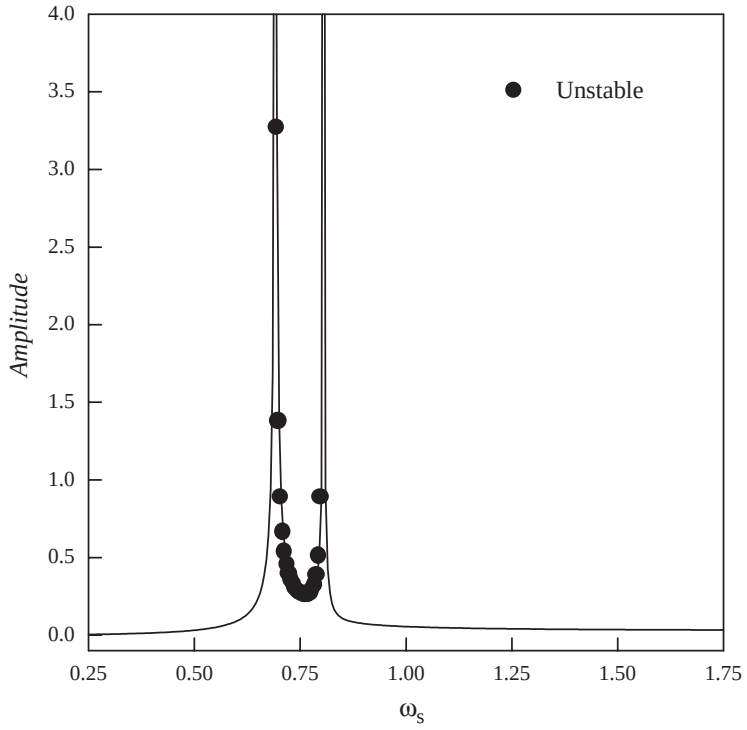

Fig. 8. SSFR of the blade second mode. $\varepsilon = 1$, $\gamma = 1$, $\zeta = 0.05$. ———SSFR; ● unstable vibrations.

$$M_{41} = 2C\varepsilon\gamma\omega_s^2,$$

$$M_{44} = 1 + \frac{\omega_s^2}{4}\{4C - 4\gamma^2 + \varepsilon^2(3C\gamma^2 - \gamma^2 - 1)\},$$

$$M_{45} = 2M_{23},$$

$$M_{46} = M_{14},$$

$$M_{54} = -M_{45},$$

$$M_{55} = 1 + \frac{\omega_s^2}{4}\{4C - 4\gamma^2 + \varepsilon^2(C\gamma^2 - 3\gamma^2 - 3)\},$$

$$M_{57} = M_{14},$$

$$M_{61} = \frac{\varepsilon^2\omega_s^2}{4}\{1 + \gamma^2(2 + C)\},$$

$$M_{64} = M_{14},$$

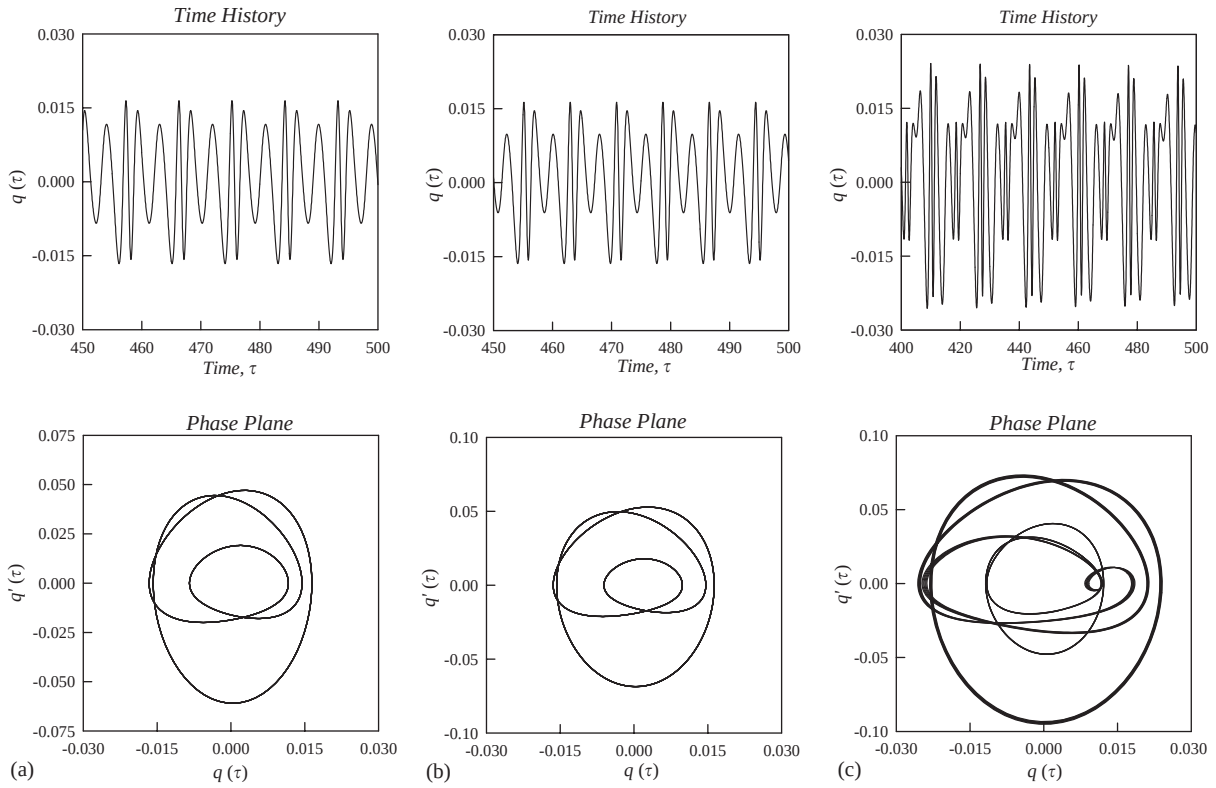

Fig. 9. Time history and phase plane of the second mode. $\varepsilon = 1$, $\gamma = 1$, $\zeta = 0.05$. (a) $\omega_s = 0.7$; (b) $\omega_s = 0.8$ and (c) $\omega_s = 0.75$.

$$M_{66} = 1 + \frac{\omega_s^2}{2}\{C(2+\varepsilon^2\gamma^2) - \varepsilon^2 - \gamma^2(8+4\varepsilon^2)\},$$

$$M_{67} = 4M_{23},$$

$$M_{75} = M_{14},$$

$$M_{76} = -M_{67},$$

$$M_{77} = 1 + \frac{\omega_s^2}{2}\{C(2-\varepsilon^2\gamma^2) - \varepsilon^2 - \gamma^2(8+4\varepsilon^2)\}. \tag{9}$$

The coefficients $A_0, A_{1/2}, B_{1/2}, A_1, B_1, A_2, B_2$ in the assumed solution (7) can be calculated by solving Eq. (8) for a given mode of blade vibration.

Now, according to Floquet Theorem, the stability of the obtained solution can be examined through evaluation the determinant of the coefficient matrix **M**. Wherein, the sustained oscillations are obtained for zero determinants, stable vibration occurs when the determinant is positive and unstable "growing" vibrations take place when the determinant is negative [11].

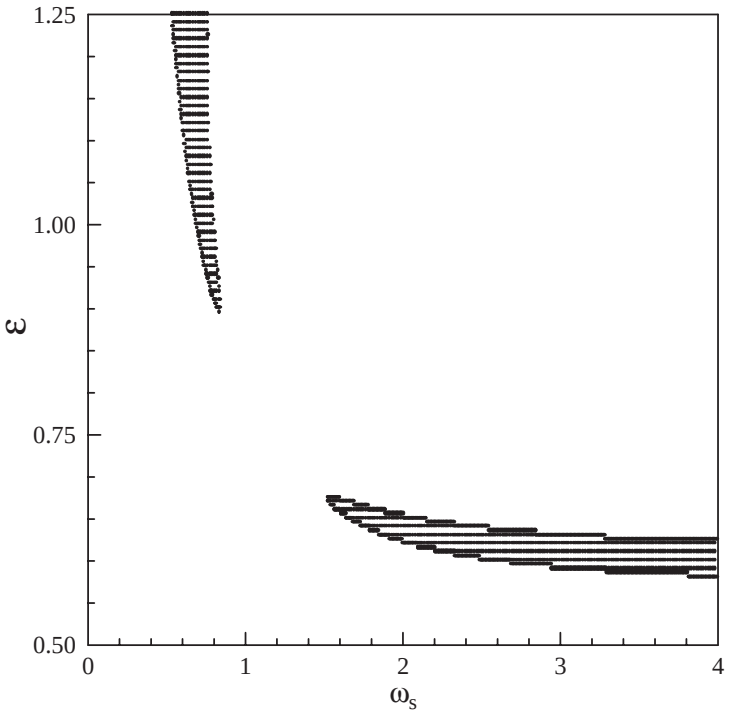

Fig. 10. Stability chart of the second mode blade bending vibrations: $\gamma = 1$ and $\zeta = 0.05$, shaded areas are unstable.

4. Results and discussion

The blade data given in Table 1 that was previously simulated in Ref. [9] is considered. The associated modal parameters obtained by integrating the expressions given in Eqs. (2) are calculated and presented in Table 2. The SSFR of the blade first bending mode, for damping ratio $\zeta = 0.1$, torsional vibration amplitude $\varepsilon = 1$ and torsional vibration frequency ratio $\gamma = 1$ is shown in Fig. 2. This steady-state response shows three peaks occurring at $\omega_s = 0.41$, 0.71 and 0.965 with the largest amplitude at $\omega_s = 0.71$. The results of evaluation the coefficient matrix determinant are included also in Fig. 2 by solid points to show unstable vibrations in the dimensionless frequency regions $0.715 \leqslant \omega_s \leqslant 0.960$ and $\omega_s \geqslant 1.225$. To check the blade stable and unstable vibration regions, Eq. (5) is integrated numerically at several points selected from Fig. 2. Typical blade first mode vibrations in the predicted stable ($\omega_s = 0.71$) and unstable ($\omega_s = 0.96$) are shown in Figs. 3a and b, respectively. The results of numerical integration in the form of blade first mode vibration amplitude and its associated phase plane plot are shown in Fig. 3. Excellent agreement between the numerical integration and HB solution can be observed.

Directed by the observation of different amplitudes at the resonance points, in Fig. 2 the effect of damping is further investigated by solving for different damping ratios ζ, and the steady-state solution is given in Fig. 4. Wherein, the damping played a prominent role at first resonance $\omega_s = 0.41$ and relatively negligible effect can be observed at the second resonance ($\omega_s = 0.71$). At the third very narrow resonance, $\omega_s = 0.965$, damping played an inverse role, i.e. amplitude

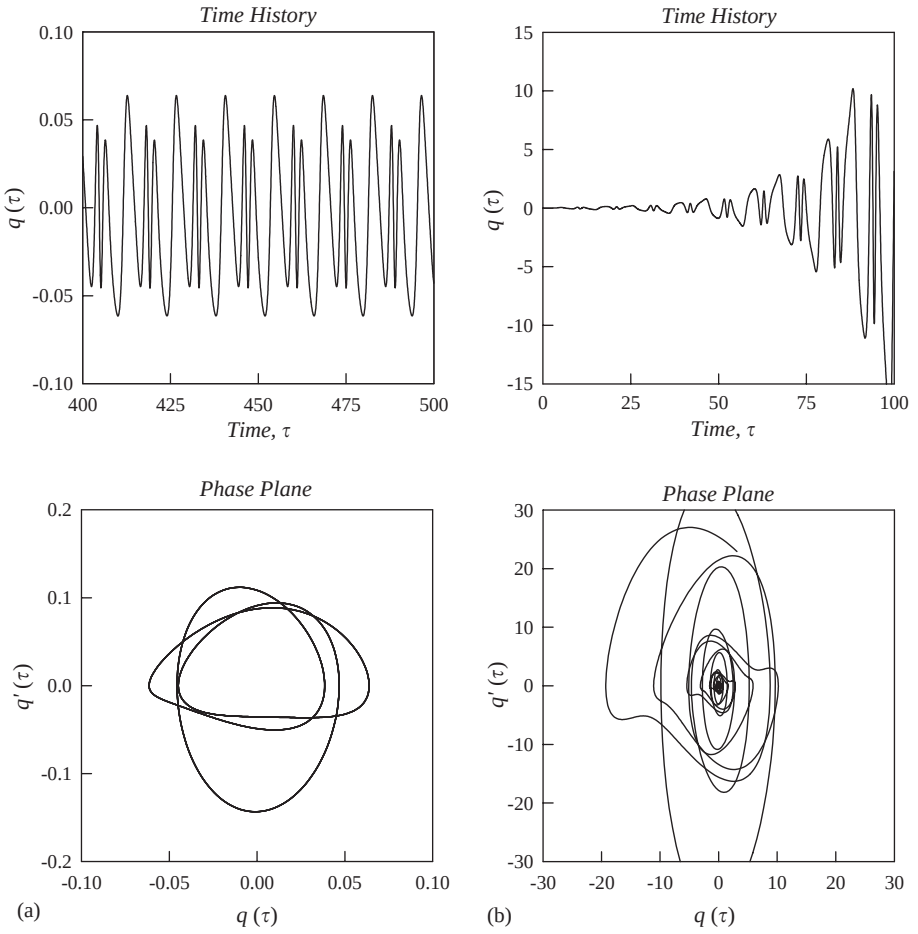

Fig. 11. Time history and phase plane of the second mode. $\zeta = 0.05$. (a) $\varepsilon = 1.5$, $\gamma = 1$, $\omega_s = 0.4$; (b) $\varepsilon = 1.5$, $\gamma = 1$, $\omega_s = 0.6$; (c) $\varepsilon = 0.6$, $\gamma = 1$, $\omega_s = 3.0$; (d) $\varepsilon = 0.7$, $\gamma = 1$, $\omega_s = 3.0$ and (e) $\varepsilon = 0.8$, $\gamma = 1$, $\omega_s = 3.0$.

increases with increasing the damping ratio ζ, with no third resonance for $\zeta = 0$ case. The explanation of this unexpected behavior is not straight forward, but it can be referred to the harmonic interactions in Eq. (5) coefficients. In addition the effect of variation of damping ratios ζ on the unstable vibrations was also studied and the results of examining the determinant of the coefficient matrix have shown that the unstable region ($0.715 \leqslant \omega_s \leqslant 0.960$) is the same for all values of ζ and one unstable point at $\omega_s = 0.41$ is found only for $\zeta = 0$.

To investigate the effect of torsional vibration strength on the blade first mode vibration, the HB solution is obtained over a wide range of ε and ω_s and the determinant of coefficient matrix is found. The regions of stable and unstable vibrations are shown in Fig. 5. Wherein narrow shaded region represents unstable vibration for a combination of ε and ω_s. Moreover, the higher amplitudes of torsional vibrations ε produce unstable vibrations for wide range of torsional vibration excitation frequencies. The effect of torsional vibration frequency to rotating speed ratio γ on the first mode vibration stability is investigated and shown in Fig. 6, Shaded regions show

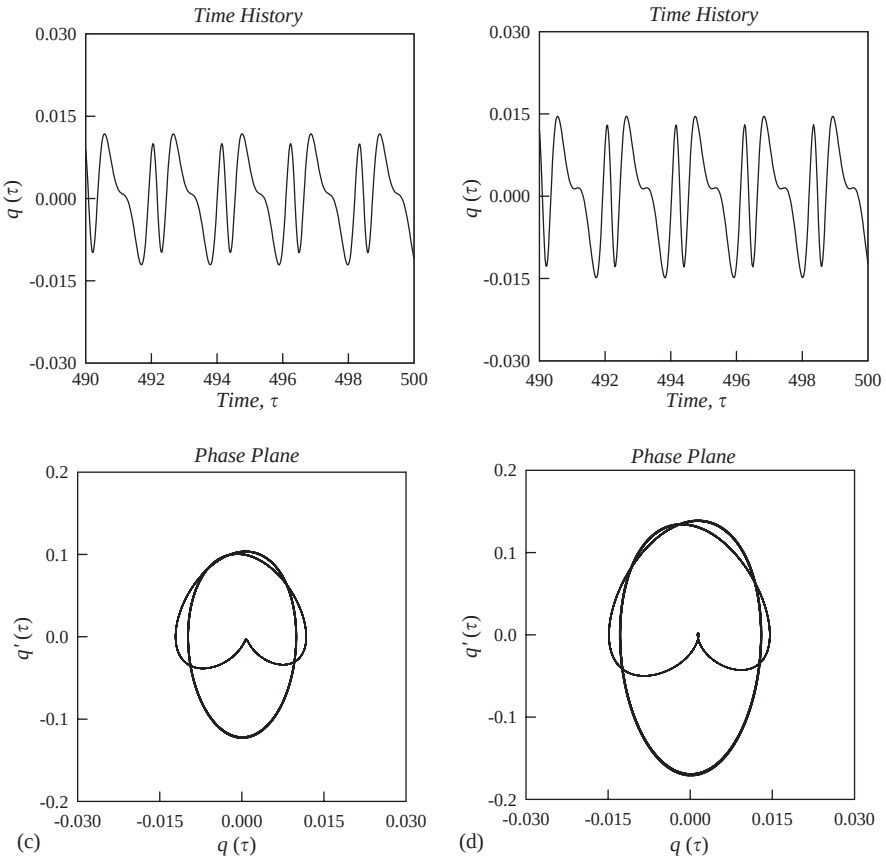

Fig. 11. (*Continued*)

unstable vibrations. Stable and unstable regions shown in Figs. 5 and 6 are verified for some selected points by numerical integrations as shown in Fig. 7. Similar treatment for the blade second vibration mode is shown in Fig. 8, for $\zeta = 0.05$, $\varepsilon = 1$ and $\gamma = 1$. The frequency response shows two peaks at $\omega_s = 0.69$ and 0.805 with unstable vibrations between the two peaks. In Fig. 9, some numerical simulations are shown for some values of ω_s selected from the unstable region between the peaks in Fig. 8. Results for the variation of ε and its effect on the stability of the second mode vibration are shown in Fig. 10. Two narrow shaded unstable areas in the $\varepsilon - \omega_s$ plane are shown. Finally, results of numerical integration obtained for the second mode are presented in Fig. 11.

5. Conclusions

The steady-state response of the rotating blade vibration under the main shaft torsional vibration excitation is studied using the method of harmonic balance (HB). The equation of motion is obtained from a previous study by assuming torsional vibration to occur with

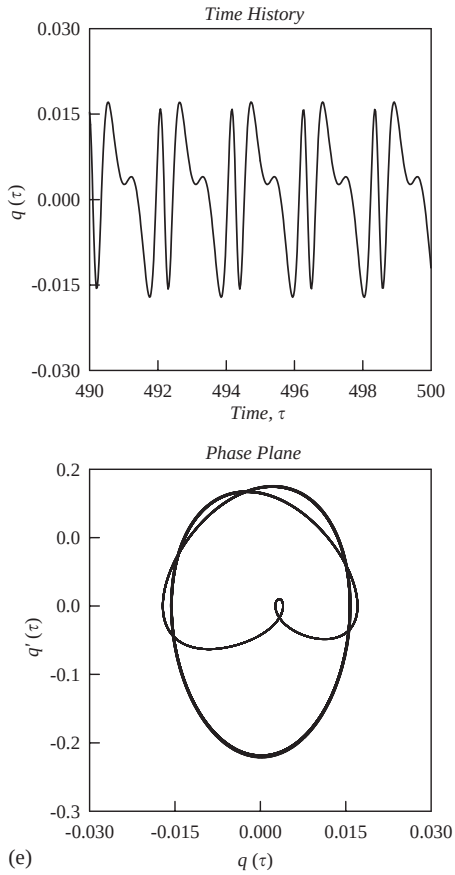

Fig. 11. (*Continued*)

controlled amplitude at a frequency related to the main rotor speed. The obtained HB solution identified stable and unstable blade vibration regions as function of the torsional vibration excitation frequency and torsional vibration amplitude. Stability maps are constructed for the first and second blade bending modes and the blades vibration stability is further verified using numerical integration. The torsional vibration amplitude was shown to play a vital role in the blade vibration stability in addition to the, role of, excitation frequency.

The produced stability maps can be used for design and diagnostic purposes. Controlled experiment to verify these findings is highly recommended.

Acknowledgments

The authors acknowledge the support of the University of Jordan. The first author appreciates the support of King Fahd University of Petroleum and Minerals. This work is supported by KFUPM Research Office under project # ME/BLADE-VIBRATION/215.

References

[1] A.V. Srinivasan, Vibrations of bladed-disk assemblies: a selected survey, *Journal of Vibration and Acoustics* 106 (1984) 165–168.
[2] E. Crawely, D. Mokadam, Stager angle dependence of the inertial and the elastic coupling in bladed disks, *Journal of Vibration and Acoustics* 106 (1984) 181–188.
[3] D. Tang, M. Wang, Coupling technique of rotor-fuselage dynamic analysis, *Journal of Vibrations and Acoustics* 106 (1984) 235–238.
[4] R. Lowely, N. Khader, Structural dynamics of rotating blade-disk assemblies coupled with flexible shaft motions, *AIAA Journal* 22 (9) (1984) 1319–1327.
[5] A. Okabe, Y. Otawara, R. Kaneko, O. Matsushita, K. Namura, An equivalent reduced modeling method and its application to shaft-blade coupled torsional vibration analysis of a turbine-generator set, *Proceedings of Institute of Mechanical Engineers* 205 (1991) 173–181.
[6] S. Huang, K. Ho, Coupled shaft-torsion and blade-bending vibrations of a rotating shaft-blade unit, *Journal of Engineering for Gas Turbines and Power* 118 (1996) 100–106.
[7] B.O. Al-Bedoor, Dynamic model of coupled shaft torsional and blade bending deformations in rotors, *Computer Methods in Applied Mechanics and Engineering* 169 (1999) 177–190.
[8] B.O. Al-Bedoor, Reduced-order nonlinear dynamic model of coupled shaft-torsional and blade-bending vibrations in rotors, *Journal of Engineering for Gas Turbines and Power* 123 (2001) 82–89.
[9] Y. Al-Nassar, B.O. Al-Bedoor, On the vibration of a rotating blade vibration on a torsionally flexible shaft, *Journal of Sound and Vibration* 259 (2002) 1237–1242.
[10] B.O. Al-Bedoor, A.A. Al-Qaisia, Analysis of rotating blade forced vibration due to torsional excitation using the method of harmonic balance, *Proceedings of ASME Pressure Vessels and Piping Conference PVP2002* 447 (2002) 17–22.
[11] A.A. AL-Qaisia, M.N. Hamdan, Bifurcation of approximate harmonic balance solutions and transition to chaos in an oscillator with inertial and elastic symmetric nonlinearities, *Journal of Sound and Vibration* 244 (2001) 453–479.